Lab on a Chip

Tunnel Dieletrophoresis for Ultra-High Precision Size-based Cell Separation

Journal:	*Lab on a Chip*
Manuscript ID	LC-ART-08-2020-000853.R2
Article Type:	Paper
Date Submitted by the Author:	17-Nov-2020
Complete List of Authors:	Kung, Yu-Chun; University of California Los Angeles, Mechanical and Aerospace Engineering Niazi, Kayvan; ImmunityBio Inc. Chiou, Pei-Yu; University of California Los Angeles

Tunnel Dieletrophoresis for Ultra-High Precision Size-based Cell Separation

Yu-Chun Kung[1,3,4], Kayvan R. Niazi[3,4], and Pei-Yu Chiou[1,2]

[1]Department of Mechanical and Aerospace Engineering, University of California at Los Angeles

[2]Department of Bioengineering, University of California at Los Angeles

[3]NanoCav LLC.

[4]ImmunityBio Inc.

Keywords : dielectrophoresis, tunable, single-stream focusing, microfluidic, cell separation

Abstract

In molecular and cellular biological research, cell isolation and sorting are required for accurate investigation of cell populations of specific physical or biological characteristics. By employing unique cell properties to distinguish between heterogeneous cell populations, rapid and accurate sorting with high efficiency is possible. Dielectrophoresis-based cell manipulation has significant promise for separation of cells based on their physical properties and is used in diverse areas ranging from cellular diagnostic to therapeutic applications. In this study, we present a microfluidic device that can achieve label-free and size-based cell separation with high size differential resolution from monocellular population or complex sample matrices. It was realized by using the tunnel dielectorphoresis (TDEP) technique to manipulate the spatial position of individual cells three dimensionally with high resolution. Cells were processed in high speed flows in high ionic strength buffers. Mixture of different sizes of polystyrene micro-particles with size difference as small as 1μm can be separated with high purity (>90%). For the first time, high-pass, low-pass, and band-pass filtering within monocellular mammalian cell population were demonstrated with tunable bandwidth as small as 3μm. In addition, leukocyte subtype separation was demonstrated by sorting monocyte out of peripheral blood mononuclear cell (PBMC) from whole blood with high purity (>85%). Its ability to deliver real-time adjustable cut-off threshold size-based cell sorting and its capability to provide arbitrary cell size pick-up band could potentially enable many research and clinical applications.

Introduction

Manipulation and sorting of biological cells has seen ever increasing widespread use in medicine, biotechnology, and cellular biology. It is often a critical first step to either separate samples into constituent cell populations/components, or to isolate a desired cell type from a complex biofluid.[1] Conventional cell isolation systems such as fluorescence-activated cell sorter (FACS)[2], magnetic activated cell sorting (MACS)[3] have demonstrated high robustness, accuracy and throughput and have high utility in industrial and lab settings. These systems achieve high throughput cell separation by labelling cells surface markers with fluorophore or magnetics beads. However, antibody-based techniques have some disadvantages related with labeling. First, labeling with secondary antibody-conjugated magnetics beads or fluorophore and primary antibodies may affect cell fate and functions, which affects

downstream analysis and efficacy of therapeutics. Second, a labeling process is often time-consuming and labor-intensive. Third, high volumes of expensive reagent is required when dealing with large sample volume. Lastly, for a practical separation and sorting application, the choice of antibodies is limited within a pool of commercially available antibodies, which in turn limits the separation targets to those cells with specific market available markers.

Label-free cell separation techniques separate cells based on physical properties of individual cells, such as, deformability[4, 5], electrical polarizability[6-12], size[13, 14], adhesion, and density[15]. Traditional label-free techniques which are widely used include micro-pore filtration[16] and density gradient centrifugation[17]. These techniques allow the separation of large numbers of desired cells in relatively simple ways. More importantly, cells separated using label-free techniques are readily available for subsequent analysis and even for therapeutic purposes. Micro-pore filtration is used as a pre-enrichment step for further cell purification, and it is especially useful in preparing single cell suspensions by removal of cell aggregates and large particles. Density gradient centrifugation can provide efficient and practical cell separation results by creating isopycnic density gradients. Cells with different densities settle to their isopycnic points via centrifugation. The biggest advantages of these two traditional approaches are simple operation and high-throughput processing capabilities. However, they can only provide rough sorting with low sorting purity and recovery rate.

To overcome certain limitations in traditional label-free cell separation technologies, microfluidic technology is expected to provide better solutions with its unique advantages[18, 19] : (1) The laminar nature of fluid flow at these scales allows confinement of cells within a narrow controlled stream line. (2) Small device dimensions allow the generation of strong mechanical, electric or magnetic fields gradient. (3) Multiple microfluidic devices can be integrated to perform separation and downstream analysis of cells seamlessly. Many new technologies in miniaturized microfluidic have been developed, which do not require expensive chemical reagents or antibody labelling thus reducing sample preparation time and cost while improving purity and yield, comprising use of pinched flow fractionation[20-22], inertial microfluidics[14, 23-29], deterministic lateral displacement[13, 30-32], dielectrophoresis[6-12, 33, 34], acoustofluidics[35-41]. These methods have pioneered many new avenues in on-chip cell separation. Recently, fundamental studies on cell size to senescence or age-related disease[42] shows potential needs for ultra-high precision size-based cell separation. However, the state-of-the-art microfluidic technologies have not been able to provide such solution.

This paper demonstrates a tunnel dielectrophoresis (TDEP) mechanism[43] for continuously tunable, three-dimensional (3D), and single-stream microparticle and cell focusing and separation in high-speed flows with ultra-high precision size-based cell and microparticle separation. The proposed microfluidic device can provide real-time and ultra-high spatial precision control for individual cells flowing in continuous flows. It is realized by fabricating a 3D heterogeneously integrated microfluidic device with two glass substrates sandwiching a thin and open PDMS channel to create a 3D tunable non-uniform electric field for lateral migration of microparticles and cells in high-speed continuous flows for up to 13cm/s. Unlike the aforementioned sorting methods, TDEP is capable of providing tunable and ultra-high precision cell size-independent 3D focusing in the upstream, and followed by high purity size-based sorting of cells and microparticles in the downstream. The 3D electric fields in upstream and downstream stages are real-time programmable to provide well-controlled cell movement in continuous flows. The upstream section provides the same spatial position and speed as a perfect reference point for individual cells entering the

downstream lateral migration stage. For the first time, size cut-off threshold can be adjusted to provide optimum sorting performance in real-time, which enable microparticles mixture to be separated with size difference as small as 1μm and high-purity separation of monocyte from isolated peripheral blood mononuclear cells (PBMC). By cascading the sorting sequence, tunable high-pass, band-pass, low-pass cell size filtration were achieved within monocellular population. Our data indicates that this method could extensively explore the flexibility and performance of label-free cell sorting technology to the next generation biological studies and applications.

Experimental Setup, Materials, and Methods

Separation Mechanism

To achieve continuous and high-resolution size-based cell sorting, two stages of particle manipulation methodologies are required as shown in Fig. 1. In the first stage, all particles, regardless of their different sizes, are three-dimensionally focused into a single-stream in a continuous flow such that different sizes of particles have exactly the same reference position entering the second stage (Fig. 1(a-ii)). In the second stage, particles migrate to a new focusing position under a new set of electric boundary condition. Due to different DEP forces acting on particles of different sizes, particles of different migration speeds can be sorted out and collected (Fig. 1(a-iii)). Fig. 1(b)(c) show the electric field pattern inside the channel when each pair of four independently tunable alternating current (a.c.) signals are applied to the quadro-electrodes along the channel to create a tunnel-shape electric field distribution with a single field minimum inside the channel. Two sets of a.c. signals $K_1(V_1, \Delta V_1)$ and $K_2(V_2, \Delta V_2)$ are applied to upstream and downstream quadro-electrode pairs correspondingly to define different electric field patterns. The TDEP is specifically designed for operation in the negative DEP mode since biological cells mainly have negative DEP responses in high ionic buffer environments. For microparticles and cells showing negative DEP responses, they will be eventually focused at the electric field minimum location regardless of their types and sizes. In addition, due to the completely perpendicular and decoupled design between the DEP and hydrodynamic forces, the focusing location is independent from the flow direction. The a.c. signal set $K_1(V_1, \Delta V_1)$ in Fig. 1(b) is used to achieve size-independent single-stream focusing. On the other hand, $K_2(V_2, \Delta V_2)$ in Fig. 1(c) is used to achieve size-dependent lateral migration of different sizes of microparticles. $(V_1, \Delta V_1)$ and $(V_2, \Delta V_2)$ are used to define the location of the electric field minimum in the upstream and downstream sections, respectively[43]. In practice, we programmed the positions of the electric field minimum to be in the middle plane, which is the plane of half channel height. In addition, the electric field minimum positions defined by $(V_1, \Delta V_1)$ and $(V_2, \Delta V_2)$ were in opposite half of the channel laterally. K_1 and K_2 are used to modulate the strength of the electric field in the upstream and downstream sections, respectively.

Dielectrophoresis refers to the interaction force between a non-uniform electric field and the dipole moment it induces on a polarizable object. The magnitude of DEP force on a spherical particle can be approximately expressed by the following equation derived based on the dipole approximation

$$\left\langle F_{DEP}(t) \right\rangle = \pi \varepsilon_m R^3 \,\mathrm{Re}\left[CM^*(\omega) \right] \times \nabla(E^2) \qquad (1)$$

where $\langle F_{DEP}(t)\rangle$ refers to the time–average DEP force, ε_m the permittivity of the medium surrounding the sphere, R the radius of the particle, ω the angular frequency of the applied electric field, and E is the magnitude of the imposed a.c. electric field. CM^* is the frequency dependent Clausius-Mossotti factor given by

$$CM^*(\omega) = \frac{\varepsilon_p^* - \varepsilon_m^*}{\varepsilon_p^* + 2\varepsilon_m^*} \tag{2}$$

where ε_p^* and ε_m^* are the complex permittivities of the particle and the medium respectively, and $\varepsilon^* = \varepsilon - j\sigma/\omega$, where ε is the permittivity and σ is the conductivity. The magnitude of DEP force is linearly proportional to the gradient of the field strength and the volume of a particle. For a particle more polarizable than the medium, the real part of its CM^* factor is bigger than zero, Re[CM^*]>0, and it experiences a positive DEP force moving it toward the strong electric field region. On the other hand, if Re[CM^*]<0, a particle experiences a negative DEP force moving it to the weak electric field region.

In order to understand the working principle of the TDEP focusing and sorting, we performed simulations using COMSOL and MATLAB [43]. A microchannel with geometry height (H=80μm), width (W=100μm), length (L=1050μm) and two sets of quadro-electrodes with 20μm in width on top and bottom surface were used as shown in Fig. 2(a). The input average flow rate flowing through the channel is 2.16×10^{-2}ml/hr. By changing the a.c. voltage signal set $K_1(V_1, \Delta V_1)$ applied on upstream quadro-electrode set, all incoming different sizes of particles are focused into a single stream with proper magnitude of the voltage set. The cross-sectional focusing position was precisely programmed at the location of electric field minimum defined by the a.c. voltage signal set (V_1, ΔV_1), as depicted in Fig. 1(b). This upstream operation is herein defined as focusing modulation (FM) mode. When the focused particles enter the downstream quadro-electrode section, another a.c. voltage signal set $K_2(V_2, \Delta V_2)$ is applied to define the new location of electric field minimum to the other side of the channel cross section as shown in Fig. 1(c). Because all incoming particles are flowing in the same cross-sectional position when entering the downstream electrode section, size dependent DEP forces (equ.1) will generate different lateral migration forces corresponding to different sizes of particles. Larger particles will migrate faster than smaller particles toward the new focusing spot. In this downstream section, we do not need to wait until larger particles to migrate to the new focusing position. By properly adjusting the magnitude of the voltage set $K_2(V_2, \Delta V_2)$, as long as the larger particles migrate across the lateral separation line, which is y=62μm in our design, then different size of particles can be separated. This stage of downstream operation is herein defined as amplitude modulation (AM) mode. The illustrative simulation particle traces of 10μm, 12μm, and 15μm of polystyrene particles flowing in suspension liquid are shown in Fig. 2(a).

In Fig. 2(c), three different sizes 10μm, 12μm, and 15μm of polystyrene particles with the same dielectric permittivity $\varepsilon_p^* = 2\varepsilon_0$ are introduced, where $\varepsilon_0 = 8.85 * 10^{-12}\mathrm{F/m}$ is the free space permittivity. In order to focus randomly distributed input particle positions into a single-stream in FM section, different sizes of particles entered the channel at different initial coordinates. The FM a.c. voltage set is $K_1(V_1, \Delta V_1)$ = 6*(5V, 2V) at frequency f = 1MHz. The conductivity of the surrounding medium in the channel is $\sigma_m = 1S/m$ with its $\varepsilon_m^* = 80\varepsilon_0 - j/\omega$, where $\omega = 2\pi f$. On the other hand, the AM a.c. voltage set is $K_2(V_2,$

ΔV_2) = 1.2*(5V, 2V) at frequency f = 1MHz. As we can see in Fig. 2(c), all different sizes of particles are focused at lateral and vertical positions of $y = 29.1\mu m$ and $z = 40\mu m$ in FM section, respectively. When entering the downstream AM section, all particles start to migrate laterally toward the new electric field minimum, which is programmed to locate at lateral and vertical positions of $y = 70.9\mu m$ and $z = 40\mu m$, respectively. Within this section, size-dependent lateral migration takes effective, and results in the different trajectories of 10μm, 12μm, and 15μm of polystyrene particles. In our microchannel design, the separation line at the downstream branching is located at $y = 62\mu m$. As a result, as long as the larger particle population of interests migrate beyond the separation line at the branching, size-based separation is achieved. Fig. 2(b) shows the maximum particle separation between three different mixtures of polystyrene particles, which are $9\mu m + 10\mu m$, $10\mu m + 12\mu m$, and $10\mu m + 15\mu m$. Under different FM conditions, the maximum particle separation distance increases as the electric field minimum position is programmed closer to the channel wall. In this simulation (V_2, ΔV_2) is fixed at (5V, 2V). K_1 is used to make sure that all the particles are focused at the same cross-sectional location under different FM conditions. When a FM condition is chosen, the maximum particle separation is determined by changing the K_2 values to keep lateral position of larger particles > 62μm and smaller particle < 62μm. As we can see, even with only 1μm size difference between 9μm and 10μm particles, we can obtain over 2μm separation distance. Which is only possible with well-controlled 3D programmable electric field and upstream 3D tight particle focusing. (video S4, Supplement Information) shows the simulated particle trajectories discussed above. To save the computation time, the channel length was shortened 50 times compared to the real 5 cm long TDEP channel used in our experiments. We also make corresponding flow rate reduction from 0.3ml/hr used in the experiment to 0.0216 ml/hr in the simulation model in order to show particle focusing and sorting behaviors in the same field of view.

Device fabrication and experimental setup

Fig. 1(d) shows the device used in our study. The fabrication process is similar to our prior work and is detailed in the supplementary materials (Fig. S1, Supporting Information). [43] Stripe electrodes are laid out on both glass slides (70mm x 22mm x 1mm) and cover slips (60mm x 22mm x 100μm). A PDMS thin film with open microchannels 100μm in width and 83μm in height[44] is aligned and transferred to the glass slides with patterned electrodes by standard oxygen plasma treatment. As shown in Fig. 1(e-g), the microchannel is aligned with the stripe electrodes along the 50mm-long straight channel from upstream (Fig. 1(e)) to downstream (Fig. 1(g)) portions. From Fig. 1(f), we can see the gap between the FM and AM stripe electrodes. Then, the top cover slip with the patterned stripe electrodes side facing down is aligned and bonded with the previously transferred substrate by oxygen plasma. This results in a device cross-section structure as glass slide → electrode → open microchannel → electrode → cover slip. Electrodes are laid out to provide DEP forces perpendicular to the hydrodynamic flow in the channel. This completely decouples the hydrodynamic forces from the DEP forces on particles and cells. A key feature of TDEP is its long DEP interaction length that give cells sufficient time to migrate to target cross section locations. In TDEP, the DEP interaction length is 5cm compared to prior DEP electrodes that provide interaction length typically < 1mm.[8] To generate continuous flow, two syringe pumps (KDS 210, KD scientific, Holliston, MA) were used.

To visualize the focused and sorted microparticles when TDEP device was in operation, the microfluidic device was mounted on the stage of an inverted microscope (Olympus IX73). Different sizes of polystyrene beads, 10μm(Fluoro-Max dyed green fluorescent particles, Thermo Scientific™), 9μm(Duke

Standards™ 2000 series uniform polymer particles, Thermo Scientific™), 12μm(Duke Standards™ 2000 series uniform polymer particles, Thermo Scientific™), 15μm(Duke Standards™ 2000 series uniform polymer particles, Thermo Scientific™) were mixed at different ratios and injected into the microchannel using the syringe pump. The size distributions of the 9μm, 10μm, 12μm, and 15μm particles were 9±0.4μm, 10±0.05μm, 12±0.4~0.5μm, and 14.6±0.5μm, respectively (Supplemental Information, section Explanation of particle size purity measurement). A function generator (Agilent 33210A) produced an a.c. signal that was augmented by a RF power amplifier (Electronics & Innovation, Ltd 2200L). Because each electrode on the device required different applied signal amplitude, two voltage modulation circuits (Fig. S-2) were used to supply the required different voltage combinations on FM and AM electrodes by sharing the single augmented signal. The applied a.c. signals were set to be between 100kHz - 2MHz, the excitation frequency range for TDEP operation. The cell and particle behavior in the lateral direction can be observed through the microscope using a high-speed camera (Phantom V9, Vision Research Inc.). Flow cytometer (Thermo Fisher Scientific, Attune NxT Flow Cytometer) was also used to analyze the cell and particle population after the experiments. The frame rates used in the supplement videos were between 10k~20k frames per second. As a result, it would take around 1~10ms for the particles and cells to flow across the field of view.

Experimental results

The motivation of developing TDEP is to solve two major technical barriers often encountered in DEP devices. One is the low throughput of DEP sorting and the other is the need of manipulating biological cells in low ionic strength buffers that often cause major concerns in real applications. To demonstrate the device performance, we first used three different polystyrene particle size mixtures (9μm+10μm), (10μm+12μm), and (10μm+15μm) suspended in phosphate-buffered saline (PBS) buffer with a conductivity of 1S/m and total concentration of ~10^6/ml. The PBS sheath liquid and sample suspension were simultaneously injected into the TDEP device at a total volume flow rate of 0.4ml/hr with 1:1 ratio. As a result, the overall average flow speed inside the microchannel is ~13cm/s. The augmented a.c. signal applied to the modulation circuits is $46V_{p\text{-}p}$ at 2MHz. Fig. 3 shows the microscope images of three different particle size mixtures (9μm+10μm), (10μm+12μm), and (10μm+15μm) at upstream focusing (Fig. 3 (a,d,g)), downstream migration (Fig. 3 (b,e,h)), and collection (Fig. 3 (c,f,i)) regions, respectively (video S5-7, Supplement Information). As predicted from the simulation, the TDEP device can successfully separate larger-sized population out of smaller ones in all three different size mixtures. Table 1 shows the size-based sorting results of the three different cases in Fig. 3. In Table 1, the purities were measured by flow cytometer. Only the 10μm particles are fluorescent polystyrene beads. In each set of the mixture experiment, over 300 total number of particles were analyzed. The larger particle size mixing ratio in each mixture is controlled at around 1-2% initial purity. As shown in Table 1, over 90% high purity larger particle separation results can be achieved in all different initial mixtures. DEP forces on particles are linearly proportional to the particle volume. The size's based sorting resolution can therefore be defined as the volume ratio of sorted particles. For example, volume ratio between 1μm and 2 μm particles is 8, while the ratio of 9μm and 10 μm particles is 1.7. Based on this standard, a sorter that can differentiate 9μm and 10 μm particles has higher size based sorting resolution than a sorter that can differentiate 1μm and 2 μm particles. To the best of our knowledge, the demonstrated TDEP based sorter has the highest size sorting resolution compared to prior microfluidics platforms.

The histograms of particle positions at locations in Fig. 1(ii) and Fig. 1(iii) for these three mixtures are shown in Fig. 4. The size-independent focusing in the upstream with less than 0.2 μm standard variation (Fig. 4(a, b, c)) of all four sizes of particles is the key to high purity sorting of particles with only 1 μm difference in size. Due to the laminar flow nature in microfluidics, the flow rate ratio between the collection (larger particles) and the waste (smaller particles) channels is around 0.62. In other words, the downstream lateral separation line is located at 62μm. As a result, as long as the separation of different sizes of particles can completely fall on either side of the blue dashed separation lines ($y = 62\mu m$) in Fig. 4(d, e, f), size-based particle sorting can be achieved.

HL60 (Human promyelocytic leukemia cells) cell line (CCL-240™, ATCC®) was used for lowpass, bandpass, and highpass filtering for cell size selection. As can be seen in Fig. 5(a), the size distribution of original HL60 culture can range from 8μm to 20μm, in which most of the cell sizes fall between 10μm to 14μm. Based on the particle separation data above, TDEP separation device can provide sharp and adjustable particle size cutoff threshold. In order to selectively pick up a specific size band, TDEP was used by running larger and smaller size cut-off threshold sequentially. HL60 cells were cultured using standard protocols and were suspended in buffer solution made of 0.1 x PBS (V/V) (diluted with an isotonic buffer of 8.5% sucrose and 0.3% dextrose) supplemented with 1% (W/V) BSA (Fraction V, Sigma-Aldrich). The overall conductivity of the buffer solution was 0.1S/m, which was used to maintain cell viability while higher $K_{1,2}$ values were applied during the TDEP sorting experiments. HL60 concentration in the input sample suspension was prepared at ~$2x10^6$/ml. The procedure used for determining cell sizes in this study can be found in Supplemental Information, section Cell size determination.

For the cell separation experiments, the primary cells used in this study, such as peripheral blood mononuclear cells (PBMCs) are more sensitive to the Joule heating and high current effect during TDEP operation in 1 x PBS. Although in particle separation experiments, 1 x PBS can be used during the TDEP operation without any electrolysis bubbling near the quadrupole electrodes, the purpose of using 0.1 x PBS was to reduce potential side effects on physiological functions of the processed cells.

The sheath liquid (buffer solution) and sample suspension were injected at a 1:1 ratio for a combined volume flow rate of 0.3ml/hr. The purpose of the sheath flow was to prevent cell debri and other sub-micron contaminant, which generally have very weak or no DEP responses, from flowing into the downstream collection channel. The augmented a.c. signal applied to the modulation circuits is 36Vp-p at 100kHz. ImageJ was used to analyze the true cell size through microscope images captured from cell population before and after the TDEP separation. In the FM section, incoming HL60 cells with different sizes were single-stream focused and flowed alongside the right side of the channel (Fig.5(b)). In the downstream AM section (Fig.5(c)), larger size HL60 cells migrated toward the left side laterally faster than smaller ones toward the collection channel (video S8, Supplement Information). Thus, the smaller cells flew into the waste channel. The liquid coming out from the collection and waste channel were injected into the cell culture medium.

As shown in Fig. 5(a), only 5.9% of the presort population has cell size larger than 14μm, which is the cut-off size in first-round size sorting. After the TDEP separation, over 99% of the sample from collection channel has size larger than 14μm (Fig. 5(d)), which resulted in a highpass filtering with 14μm as its cut-off threshold. Fig. 5(d-iii) shows the microscope image and histogram (Fig. 5(d), blue histogram) of the

sorted HL-60 cells in the collection channel. In the second-round of experiment, cell sample collected from the waste channel was fed into the device with the same experiment setting described above, but with smaller AM voltage amplitude. The presorted size distribution has 34.7% smaller than 11μm, which is the new cut-off size in second-round size sorting. After the TDEP separation, only 8.5% of the sample from collection channel was smaller than 11μm, which resulted in a 3μm bandpass filtering size distribution with 11μm and 14μm as its lower and higher cut-off thresholds, respectively. Fig. 5(d-ii) shows the microscope image and histogram (Fig. 5(d), yellow histogram) of the sorted HL-60 cells from the collection channel. Regarding to the sample from the waste channel, around 98% of the cell sample from the waste channel has size smaller than 11μm, which resulted in a lowpass filtering with cut-off threshold located at 11μm. Fig. 5(d-i) shows the microscope image and histogram (Fig. 5(d), green histogram) of the sorted HL-60 cells from the waste channel. Propidium iodie (PI) dye was used to measure the viability of HL-60 cells before and after the TDEP separation process with value of 86% and 79%, respectively, as shown in Fig. 5(e).

Blood plays an important role in homeostatic regulation with each of its cellular components having important therapeutic and diagnostic uses. Therefore, separation of specific types of blood cells from whole blood has been of great interest to clinicians and researchers. For example, monocytes play an important role in the immune system and are responsible for phagocytizing and degrading foreign microorganisms in the body. The isolation of monocytes is important in various immunological applications such as in-vitro culture of dendritic cells. In this example, TDEP was used to separate monocyte from PBMC. PBMC was prepared by Ficoll density gradient centrifugation (Ficoll paque plus, GE Healthcare) from human whole blood (IWB1K2E10ML, Innovative Research) and suspended in DEP buffer with cell concentration of $2x10^6$/ml. T lymphocytes were stained with CD3 monoclonal antibody (APC, eBioscience™) to identify the majority of lymphocytes with smaller sizes. On the other hand, monocytes were stained with CD14 monoclonal antibody (FITC, eBioscience™) to identify the majority of PBMC with larger sizes. The cell sample was resuspended in buffer solution mentioned above with a conductivity of 0.1S/m.The sheath liquid (buffer solution mentioned above) and sample suspension were injected with total volume flow rate of 0.2ml/hr with 1:1 ratio. The augmented a.c. signal applied to the modulation circuits is 35Vp-p at 100kHz. ImageJ was used to analyze the true cell size through microscope images captured from cell population before and after the TDEP separation. Before the TDEP separation, flow cytometer (Thermo Fisher Scientific, Attune NxT Flow Cytometer) data of PBMC (Fig. 7(b)) showed that 54% of the population was T lymphocytes, 14.4% of the population was monocytes, and the rest 31.1% of the population could include B lymphocytes and natural killer cells. The nominal size distribution of monocytes are 9μm to 15μm. Whereas, lymphocyte sizes falls within 6μm to 9μm. From the microscope images (Fig. 6(a-i)), Fig. 6(a) also showed that 11% of the population has cell sizes larger than 8.5μm, which could represent the monocyte population. With the buffer used in the TDEP process, the real part of the Clausius-Mossotti factor versus excitation frequency is shown in Fig. S-3. Under 100kHz excitation frequency, Re[CM^*] of the T lymphocyte, B lymphocyte, and monocyte are -0.4810, -0.4635, and -0.4442, respectively[45], and their differences are small. The DEP responses of these cells are dominated by the size factor.

In the FM section, incoming PBMCs with different sizes were single-stream focused and flowed alongside the left side of the channel (Fig.6(d)). In the downstream AM section (Fig.6(c)), larger size monocytes migrated toward the right side laterally faster than smaller lymphocytes toward the collection channel (video S9, Supplement Information). Fig. 7(d) shows the flow cytometer data of the sample

collected from the collection channel of TDEP device. The monocyte population (CD14+) was increased from 14% to 85%, which has around 9 fold enrichment. From the microscope images (Fig. 6(b-i, ii), Fig. 6(b) also showed that 99% of the population has cell sizes larger than 8.5μm (green histogram). Fig. 7(a) shows the forward v.s. side scattering plot of PBMC before the TDEP process, in which we can clearly identify three different size distribution, small cells/debri, lymphocytes, and larger cells. Fig. 7(c) shows the forward v.s. side scattering plot of the sample collected from the collection channel, in which the small cells/debri and lymphocyte population were obviously eliminated. Fig. 7(e) shows the forward v.s. side scattering plot of the sample collected from waste channel, in which retained the population of small cells/debri and lymhpocytes. Propidium iodie (PI) dye was also used to measure the viability of PBMCs before and after the TDEP separation process with value of 94% and 89%, respectively (Fig. 6(e)).

Conclusion

In summary, we present ultra-high precision size-based cell separation platform using TDEP technology. The TDEP process has two major steps in sequence. The upstream FM mode performs size-independent single-stream cell focusing to create the programmable reference point (a.c. voltage signal set $K_1(V_1, \Delta V_1)$) for downstream sorting. The downstream AM mode performs size-based lateral migration by using programmable a.c. voltage signal set $K_2(V_2, \Delta V_2)$ for size-based cell migration from the reference point defined upstream. Various microspheres and cells (monocellular or heterogeneous population) separation were demonstrated for the as small as 1μm particle size sorting resolution, low-pass, band-pass(bandwidth as small as 3μm), high-pass monocular size sorting, and specific cell type separation from heterogeneous population. Compared to prior-art DEP separation technologies, the TDEP implementation provides higher sorting throughput and precision by utilizing the long 3D quadro-electrode configuration to provide longer and continuous DEP interaction time on particles. It provides a size-independent 3D single-stream focusing that can be real-time programmed with high spatial precision for downstream sorting with high resolution.

In addition, most of the prior-art DEP microfluidic chips used 2D (single-plane) electrode designs. However, DEP force is mainly available near the electrode surface. The force drops exponentially in the vertical direction. This decreases the throughput due to the small active DEP regions in the channel. Although some prior 3D DEP electrodes have been demonstrated, the sorting principle is based on tilted electrodes and not-fully decoupled DEP and hydrodynamic forces from the flow. Therefore, the maximum particle flow speed is limited by the DEP force component along the flow direction. When a particle flows at a speed higher than what the DEP force can hold, the trap or the sorter fails. In contrast, in the TDEP device, the directions of the DEP force and the hydrodynamic viscous force from the flow are perpendicular to each other and fully decoupled (assuming no inertial flow effects introduced). Therefore, regardless of the particle flow speeds and particle sizes, all particles will migrate to the same target cross sectional location for focusing. This is the reason why particles can flow at a speed 13cm/sec in the TDEP channel while in most prior DEP sorters, particles can only flow at a speed < 1mm/sec.

References

1. C. M. Yousuff, E. T. W. Ho, I. H. K. and N. H. B. Hamid, *Micromachines*, 2017, **8**, 26.
2. A. Adan, G. Alizada, Y. Kiraz, Y. Baran and A. Nalbant, *Critical Reviews in Biotechnology*, 2017, **37**, 163-176.
3. M. Almeida, A. C. García-Montero and A. Orfao, *Pathobiology*, 2014, **81**, 261-275.

4. S. M. McFaul, B. K. Lin and H. Ma, *Lab on a Chip*, 2012, **12**, 2369-2376.
5. G. Wang, W. Mao, R. Byler, K. Patel, C. Henegar, A. Alexeev and T. Sulchek, *PLoS One*, 2013, **8**, e75901.
6. I.-F. Cheng, V. E. Froude, Y. Zhu, H.-C. Chang and H.-C. Chang, *Lab on a Chip*, 2009, **9**, 3193-3201.
7. P. R. C. Gascoyne and S. Shim, *Cancers*, 2014, **6**, 545-579.
8. U. Kim, C.-W. Shu, K. Y. Dane, P. S. Daugherty, J. Y. J. Wang and H. T. Soh, *Proceedings of the National Academy of Sciences*, 2007, **104**, 20708–20712.
9. a. J. V. M. D. Vahey, *Analytical Chemistry*, 2009, **81**, 2446-2455.
10. H.-S. Moon, K. Kwon, S.-I. Kim, H. Han, J. Sohn, S. Lee and H.-I. Jung, *Lab on a Chip*, 2011, **11**, 1118-1125.
11. H. Song, J. M. Rosano, Y. Wang, C. J. Garson, B. Prabhakarpandian, K. Pant, G. J. Klarmann, A. Perantoni, L. M. Alvarez and E. Lai, *Lab on a Chip*, 2015, **15**, 1320-1328
12. Z. Wei, X. Li, D. Zhao, H. Yan, Z. Hu, Z. Liang and Z. Li, *Analytical Chemistry*, 2014, **86**, 10215-10222.
13. K. Loutherback, J. D'Silva, L. Liu, A. Wu, R. H. Austin and J. C. Sturm, *AIP Advance*, 2012, **2**, 042107.
14. M. E. Warkiani, B. L. Khoo, L. Wu, A. K. P. Tay, A. A. S. Bhagat, J. Han and C. T. Lim, *Nature Protocols*, 2016, **11**, 134-148.
15. N. Norouzi, H. C. Bhakta and W. H. Grover, *PLoS One*, 2017, **12**, e0180520.
16. H. M. Ji, V. Samper, Y. Chen, C. K. Heng, T. M. Lim and L. Yobas, *Biomedical Microdevices*, 2008, **10**, pp 251–257.
17. S. O. Majekodunmi, *American Journal of Biomedical Engineering*, 2015, **5**, 67-78.
18. Y. Chen, T.-H. Wu, Y.-C. Kung, M. A. Teitell and P.-Y. Chiou, *Analyst*, 2013, **138**, 7308-7315
19. Y.-J. Fan, Y.-C. Wu, Y. Chen, Y.-C. Kung, T.-H. Wu, K.-W. Huang, H.-J. Sheen and P.-Y. Chiou, *Biomicrofluidics*, 2013, **7**, 044121.
20. J. Takagi, M. Yamada, M. Yasuda and M. Seki, *Lab on a Chip*, 2005, **5**, 778-784.
21. M. Yamada, M. Nakashima and M. Seki, *Analytical Chemistry*, 2004, **76**, 5465-5471.
22. H. Zhang and D. Lyden, *Nature Protocols*, 2019, **14**, 1027-1053.
23. A. A. S. Bhagat, H. W. Hou, L. D. Li, C. T. Lim and J. Han, *Lab on a Chip*, 2011, **11**, 1870-1878.
24. M. Dhar, J. Wong, A. Karimi, J. Che, C. Renier, M. Matsumoto, M. Triboulet, E. B. Garon, J. W. Goldman, M. B. Rettig, S. S. Jeffrey, R. P. Kulkarni, E. Sollier and D. D. Carlo, *Biomicrofluidics*, 2015, **9**, 064116.
25. A. J. Mach, J. H. Kim, A. Arshi, S. C. Hur and D. D. Carlo, *Lab on a Chip*, 2011, **11**, 2827-2834.
26. J. Sun, M. Li, C. Liu, Y. Zhang, D. Liu, W. Liu, G. Hu and X. Jiang, *Lab on a Chip*, 2012, **12**, 3952-3960.
27. Z. Wu, Y. Chen, M. Wang and A. J. Chung, *Lab on a Chip*, 2016, **16**, 532-542.
28. X. Zhang, N. Xiang, W. Tang, D. Huang, X. Wang, H. Yi and Z. Ni, *Lab on a Chip*, 2015, **15**, 3473-3480.
29. D. D. Carlo, J. F. Edd, K. J. Humphry, H. A. Stone and M. Toner, *Physical Review Letters*, 2009, **102**, 94503.
30. L. R. Huang, E. C. Cox, R. H. Austin and J. C. Sturm, *Science*, 2004, **304**, 987-990.
31. K. K. Zeming, N. V. Thakor, Y. Zhang and C.-H. Chen, *Lab on a Chip*, 2016, **16**, 75-85.
32. K. K. Zeming, S. Ranjan and Y. Zhang, *Nature Communication*, 2013, **4**.
33. S. Yan, J. Zhang, Y. Yuan, G. Lovrecz, G. Alici, H. Du, Y. Zhu and W. Li, *Electrophoresis*, 2015, **36**, 284-291.
34. L. Wang, L. A. Flanagan, N. L. Jeon, E. Monuki and A. P. Lee, *Lab on a Chip*, 2007, **7**, 1114-1120

35. P. Li, Z. Mao, Z. Peng, L. Zhou, Y. Chen, P.-H. Huang, C. I. Truica, J. J. Drabick, W. S. El-Deiry, M. Dao, S. Suresh and T. J. Huang, *Proceedings of the National Academy of Sciences*, 2015, **112**, 4970-4975.
36. G. Destgeer, K.-H. Lee, J.-H. Jung, A. A and H.-J. Sung, *Lab on a Chip*, 2013, **13**, 4210-4216
37. P. Augustsson, J. T. Karlsen, H.-W. Su, H. Bruus and J. Voldman, *Nature Communication*, 2016, **7**.
38. S.-Y. Jung, T. Notton, E. Fong, M. Shusteff and L. S. Weinberger, *Lab on a Chip*, 2015, **15**, 1000-1003.
39. J. Nam, Y. Lee and S. Shin, *Microfluidics and Nanofluidics*, 2011, **11**, 317–326.
40. Z. Tian, Z. Wang, P. Zhang, T. D. Naquin, J. Mai, Y. Wu, S. Yang, Y. Gu, H. Bachman, Y. Liang, Z. Yu and T. J. Huang1, *Science Advances*, 2020, **6**, eabb0494.
41. P. Zhang, C. Chen, X. Su, J. Mai, Y. Gu, Z. Tian, H. Zhu, Z. Zhong, H. Fu, S. Yang, K. Chakrabarty and T. J. Huang, *Science Advances*, 2020, **6**, eaba0606.
42. G. E. Neurohr, R. L. Terry, J. Lengefeld, M. Bonney, G. P. Brittingham, F. Moretto, T. P. Miettinen, L. P. Vaites, L. M. Soares, J. A. Paulo, J. W. Harper, S. Buratowski, S. Manalis, F. J. v. Werven, L. J. Holt and A. Amon, *Cell*, 2019, **176**, 1083-1097.
43. Y.-C. Kung, K.-W. Huang, W. Chong and P.-Y. Chiou, *Small*, 2016, **12**, 4343–4348.
44. Y.-C. Kung, K.-W. Huang, Y.-J. Fan and P.-Y. Chiou, *Lab on a Chip*, 2015, **15**, 1861-1868
45. Y.-D. J. S.-I. Han, and K.-H. Han, *Analyst*, 2013, **138**, 1529-1537.

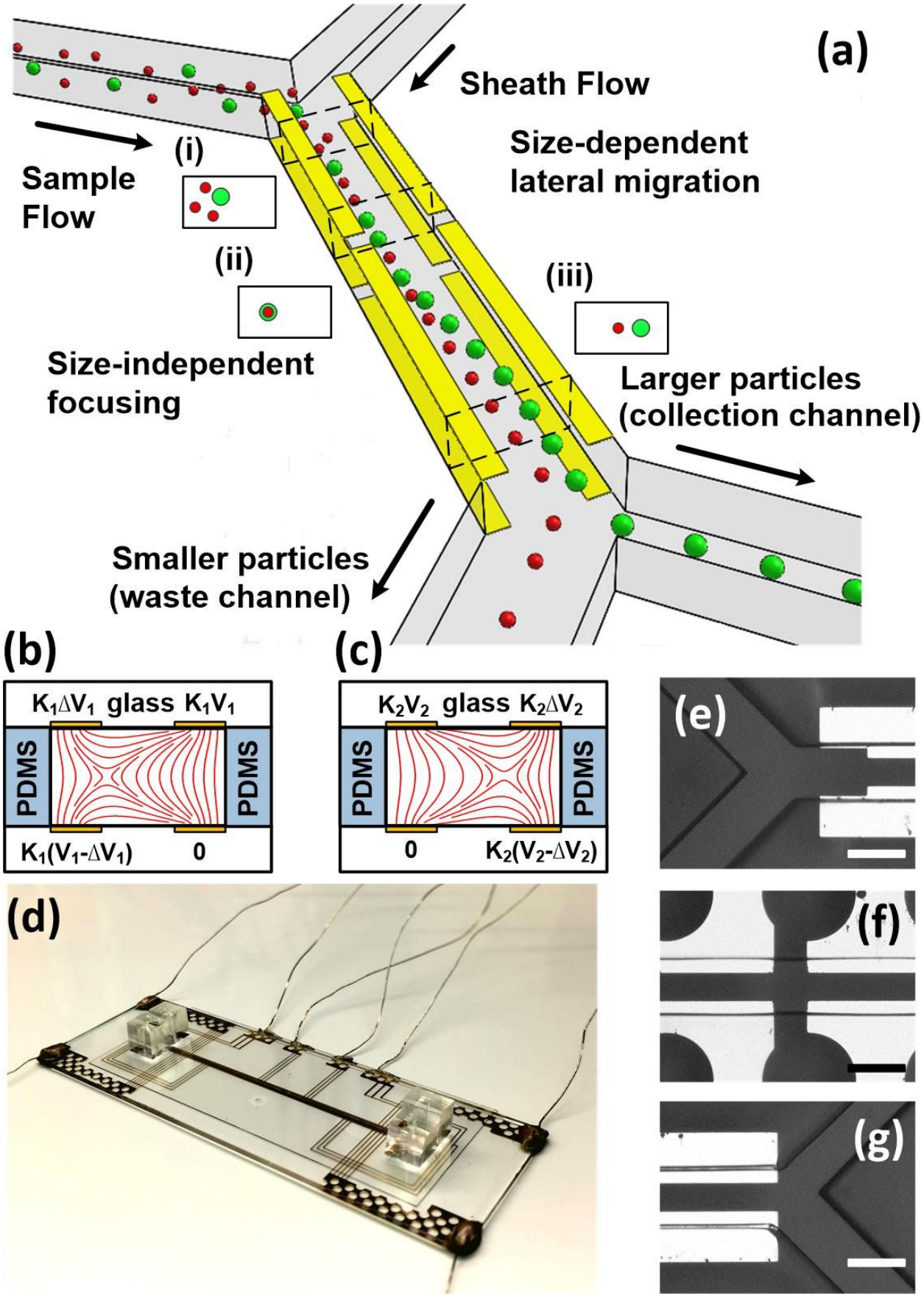
(a)
Sheath Flow
Size-dependent
lateral migration
(i)
Sample
Flow
(ii)
(iii)
Size-independent
focusing
Larger particles
(collection channel)
Smaller particles
(waste channel)
(b)
K1ΔV1 glass K1V1
PDMS
PDMS
K1(V1-ΔV1)
0
(c)
K2V2 glass K2ΔV2
PDMS
PDMS
0
K2(V2-ΔV2)
(d)
(e)
(f)
(g)

Fig. 1 Continuous and high-resolution size-based TDEP cell sorting. (a) Schematic of a TDEP separation platform. In the first stage, all particles, regardless of their different sizes, are three-dimensionally focused into a single-stream in a continuous flow such that different sizes of particles have exactly the same reference position entering the second stage (a-ii). In the second stage, particles migrate to a new focusing position under a new set of electric boundary condition. Due to different DEP forces acting on particles of different sizes, particles of different migration speeds can be sorted out and collected (a-iii). (b) and (c) show the electric field pattern inside the channel when each pair of four independently tunable alternating current (a.c.) signals. (d) A fabricated TDEP device used in this study. (e-g), the microchannel is aligned with the stripe electrodes along the 50mm-long straight channel from upstream (e), midstream (f) to downstream (g) portions. The scale bars in (e-g) are 100μm

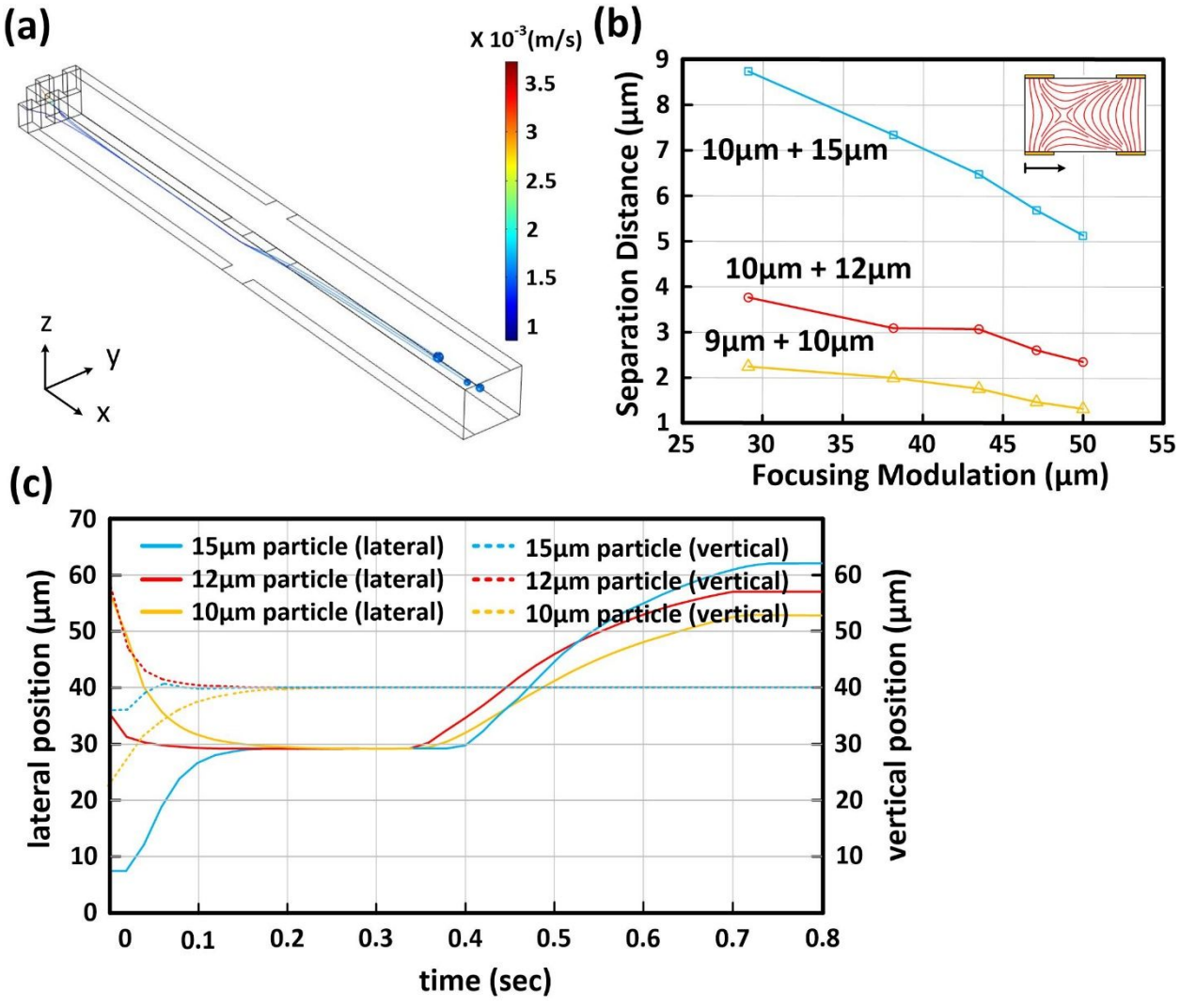

Fig. 2 Simulated particle traces of 10μm, 12μm, and 15μm of polystyrene particles flowing in suspension liquid, in which a microchannel with geometry height (H=80μm), width (W=100μm), length (L=1050μm) and two sets of quadro-electrodes with 20μm in width on top and bottom

surface were used. All incoming particles are flowing in the same cross-sectional position (FM section) when entering the downstream electrode section (AM section). In the downstream section, larger particles will migrate faster than smaller particles toward the new focusing spot. (c), all different sizes of particles are focused at lateral and vertical positions of y=29.1μm and z=40μm in the FM section, respectively. When entering the downstream AM section, all particles start to migrate laterally toward the new electric field minimum, which is programmed to locate at lateral and vertical positions of y=70.9μm and z=40μm, respectively. Within this section, size-dependent lateral migration takes effective, and results in the different trajectories of 10μm, 12μm, and 15μm of polystyrene particles. (b) shows the maximum particle separation between three different polystyrene particles mixtures, 9μm+10μm, 10μm+12μm, and 10μm+15μm.

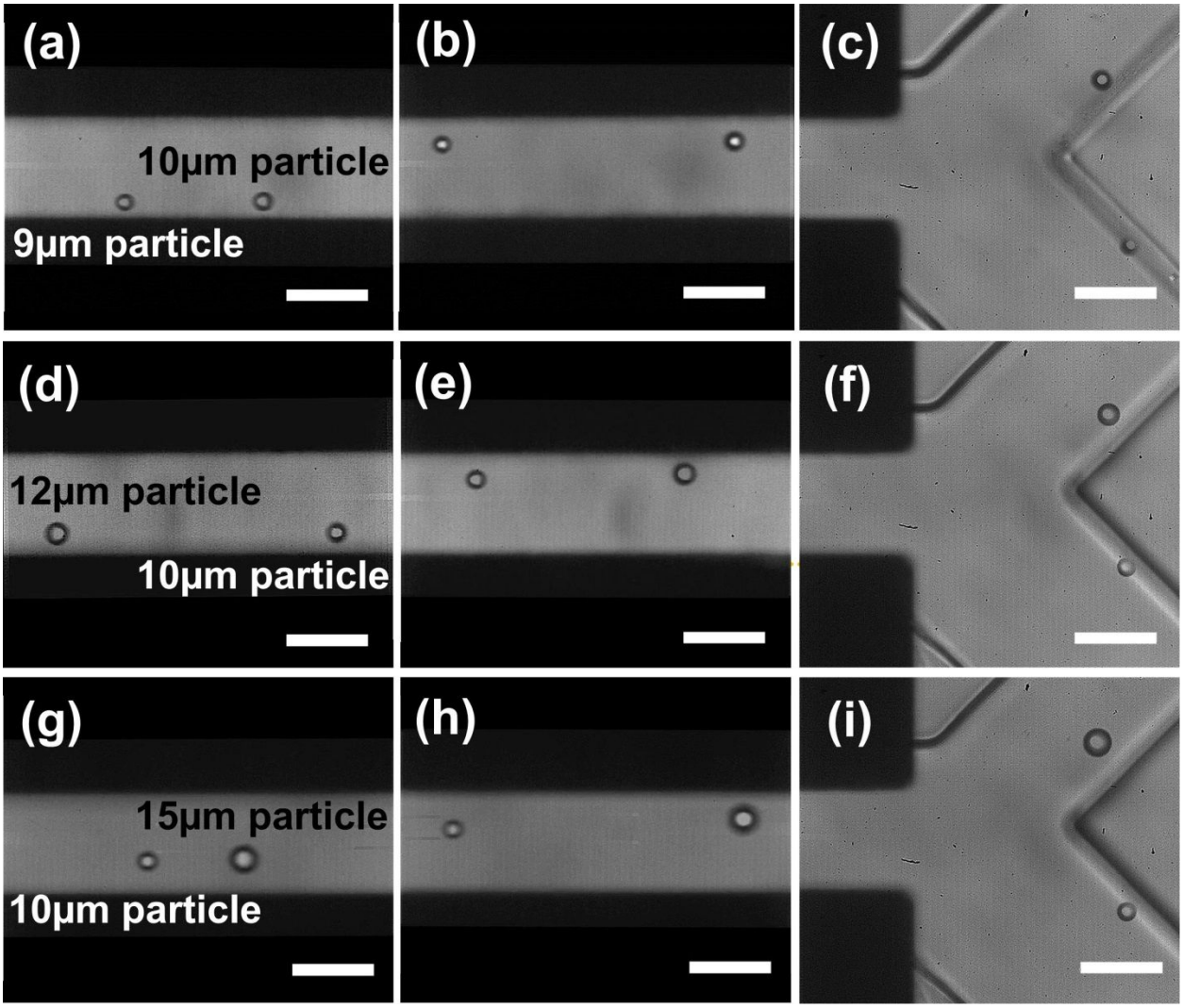

Fig. 3 The microscope images of three different particle size mixtures (9μm+10μm), (10μm+12μm), and (10μm+15μm) at upstream focusing (a,d,g), downstream migration (b,e,h), and collection (c,f,i) regions, respectively. The scale bar is 50μm.

Beads Mix	Before Sort Purity	After Sort Purity
9μm + 10μm	1.2%	94.2%
10μm + 12μm	1.8%	98.8%
10μm + 15μm	1.6%	99.1%

Table 1 Size-based microparticle sorting results (purity represents the concentration of larger-sized particle).

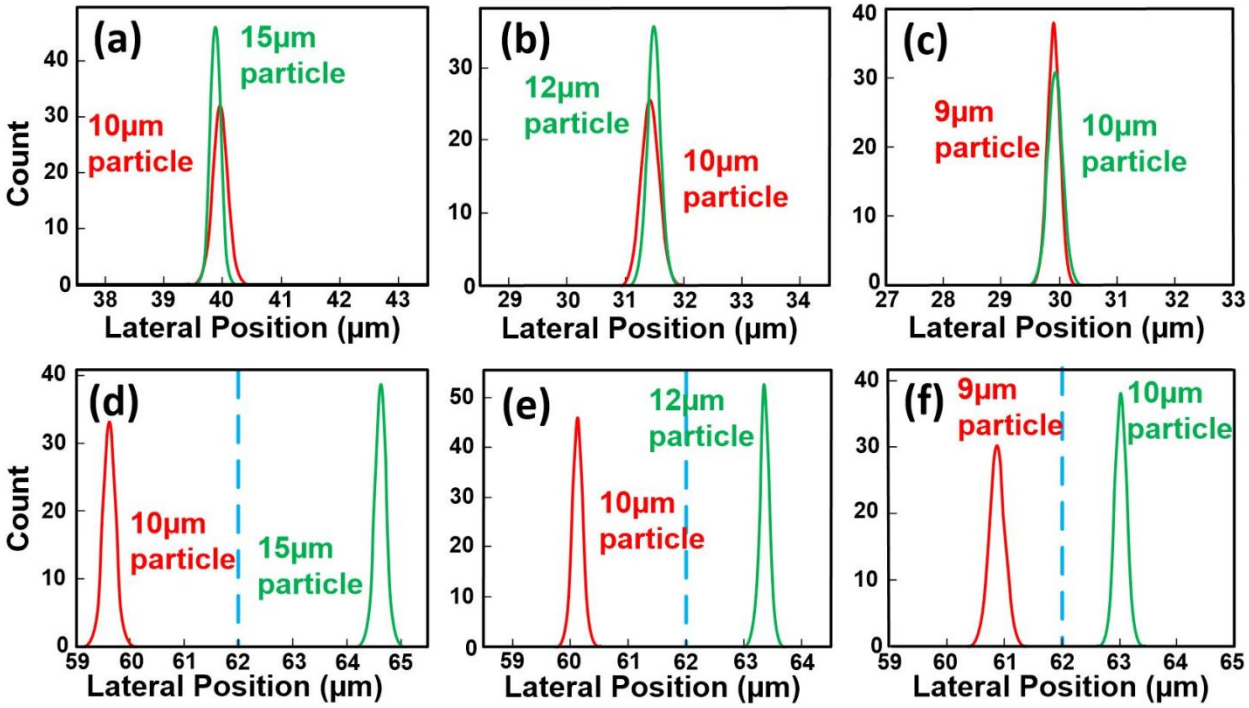

Fig. 4 Histograms of particle positions at locations in Fig. 1(ii) and Fig. 1(iii) for three particle size mixtures (9μm+10μm), (10μm+12μm), and (10μm+15μm). The size-independent focusing in the upstream with less than 0.2 μm standard variation (a, b, c) of all four sizes of particles is the key to high purity sorting of particles with only 1 μm difference in size. Due to the laminar flow nature in microfluidics, the flow rate ratio between the collection (larger particles) and the waste (smaller particles) channels is around 0.62. In other words, the downstream lateral separation line is located at 62μm. As a result, as long as the separation of different sizes of particles can completely fall on either side of the blue dashed separation lines (y=62μm) in (d, e, f), size-based particle sorting can be achieved.

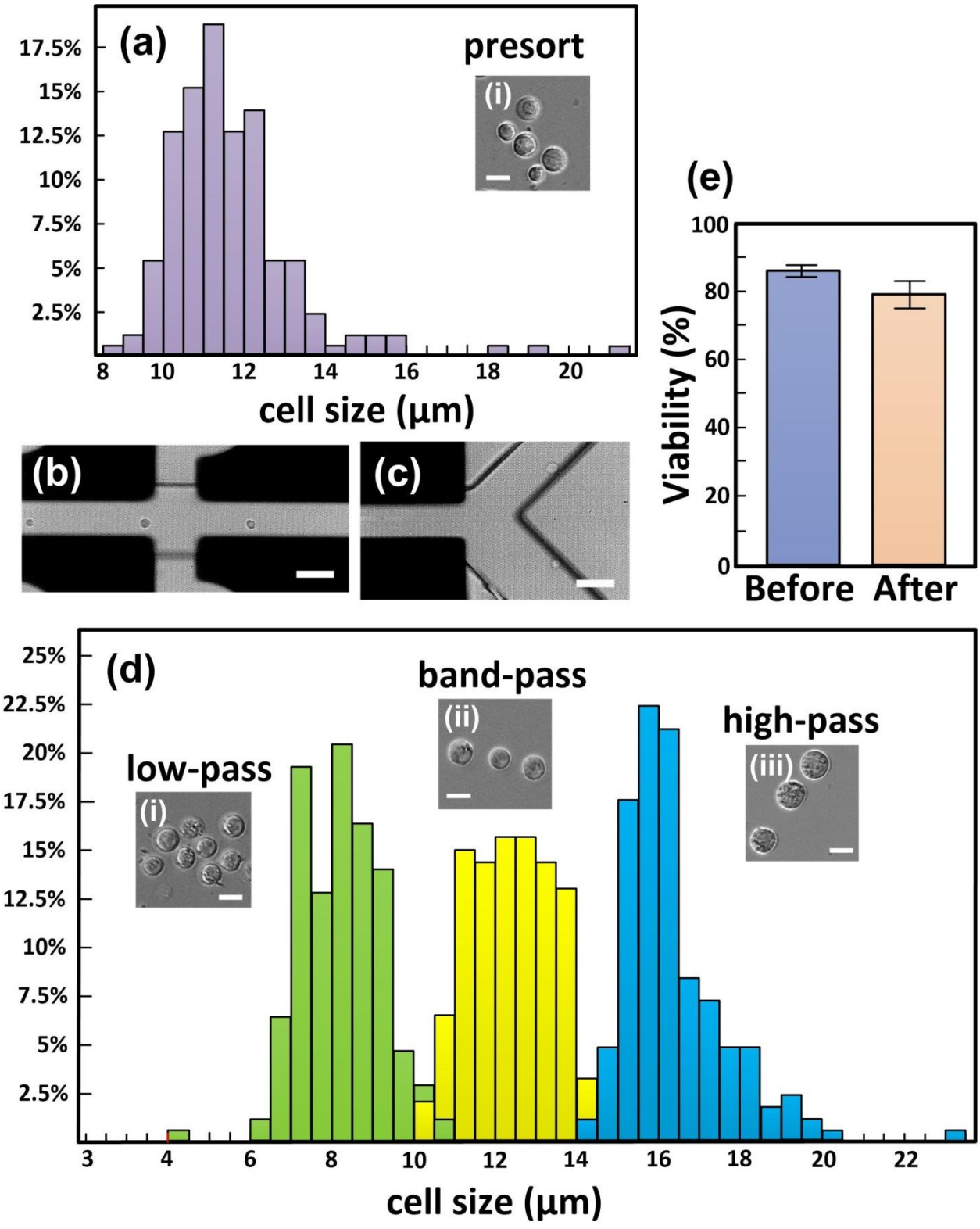

Fig. 5 (a), the size distribution of original HL60 culture can range from 8μm to 20μm, in which most of the cell sizes fall between 10μm to 14μm. (b), in the FM section, incoming HL-60 cells with different sizes were single-stream focused and flowed alongside the right side of the channel. (c), in the

downstream AM section, larger size HL-60 cells migrated toward the left side laterally faster than smaller ones toward the collection channel. Thus, the smaller cells flew into the waste channel. By cascading the size sorting process with programmed different size threshold, (d) shows the overlapped cell size distribution histograms obtained from two sequential TDEP sorting with two different size cut-off threshold settings. Two different size-cut-off thresholds were used to demonstrate low-pass (green histogram), band-pass (yellow histogram), and high-pass (blue histogram) sorting capability of TDEP technology. The bandwidth of the band-pass filter was as small as 3μm. (e) shows the viability of HL-60 cells before and after the TDEP process. The scale bars in (a,d) are 20μm, and (b,c) are 50μm

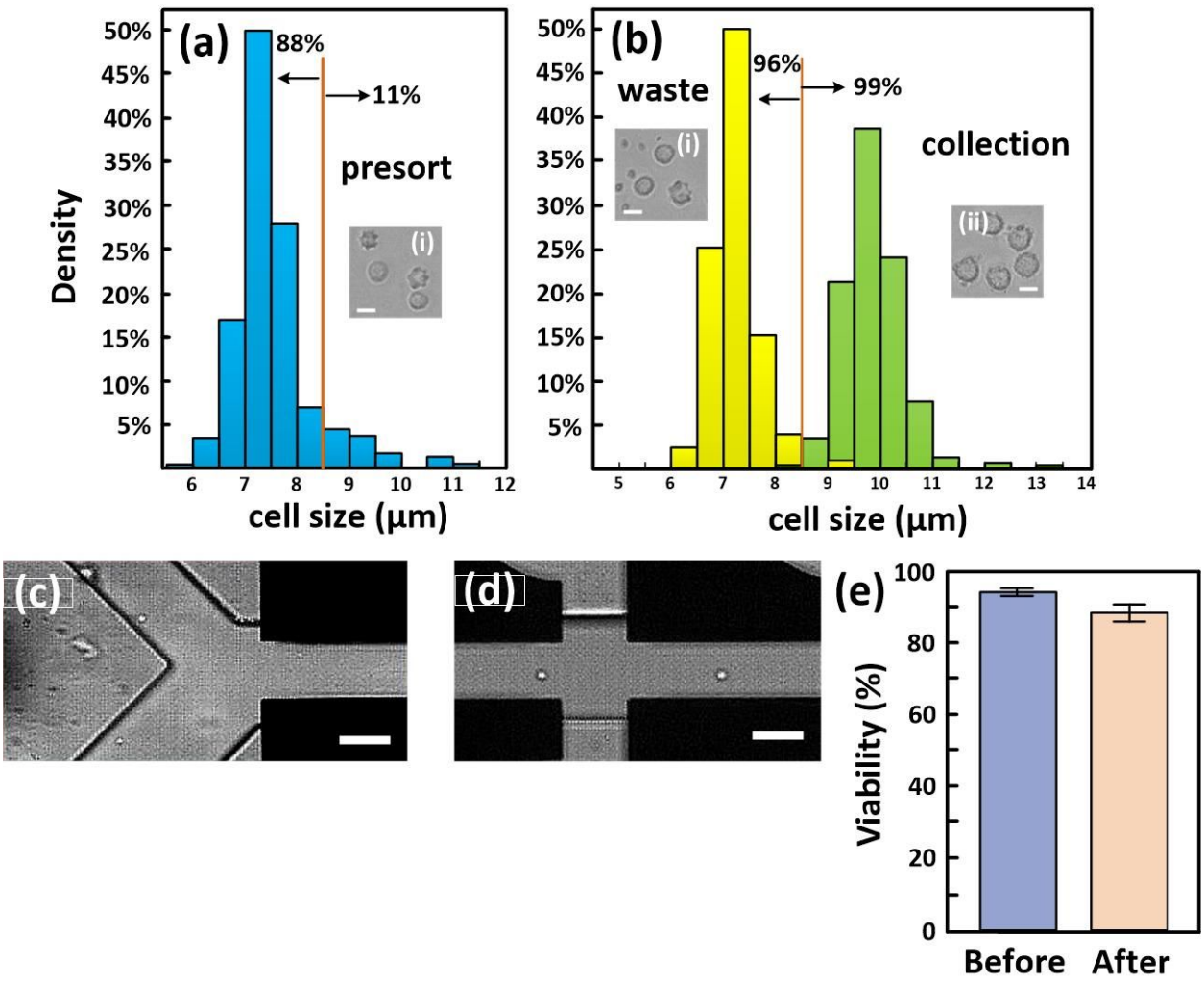

Fig. 6 (a) shows that 11% of the presort PBMC population has cell sizes larger than 8.5μm, which could represent the monocyte population. (b) shows the overlapped cell size distribution histograms obtained in TDEP PBMC sorting, from which 99% of the cell population in collection channel (green histogram) has cell sizes larger than 8.5μm after the TDEP separation process. In the FM section, incoming PBMCs with different sizes were single-stream focused and flowed alongside the left side of the channel (d). In the downstream AM section (c), larger size monocytes migrated toward the right side laterally faster than smaller lymphocytes toward the collection channel. (e) shows the viability of PBMCs before and after the TDEP process. The scale bars in (a,b) are 10μm, and (c,d) are 50μm

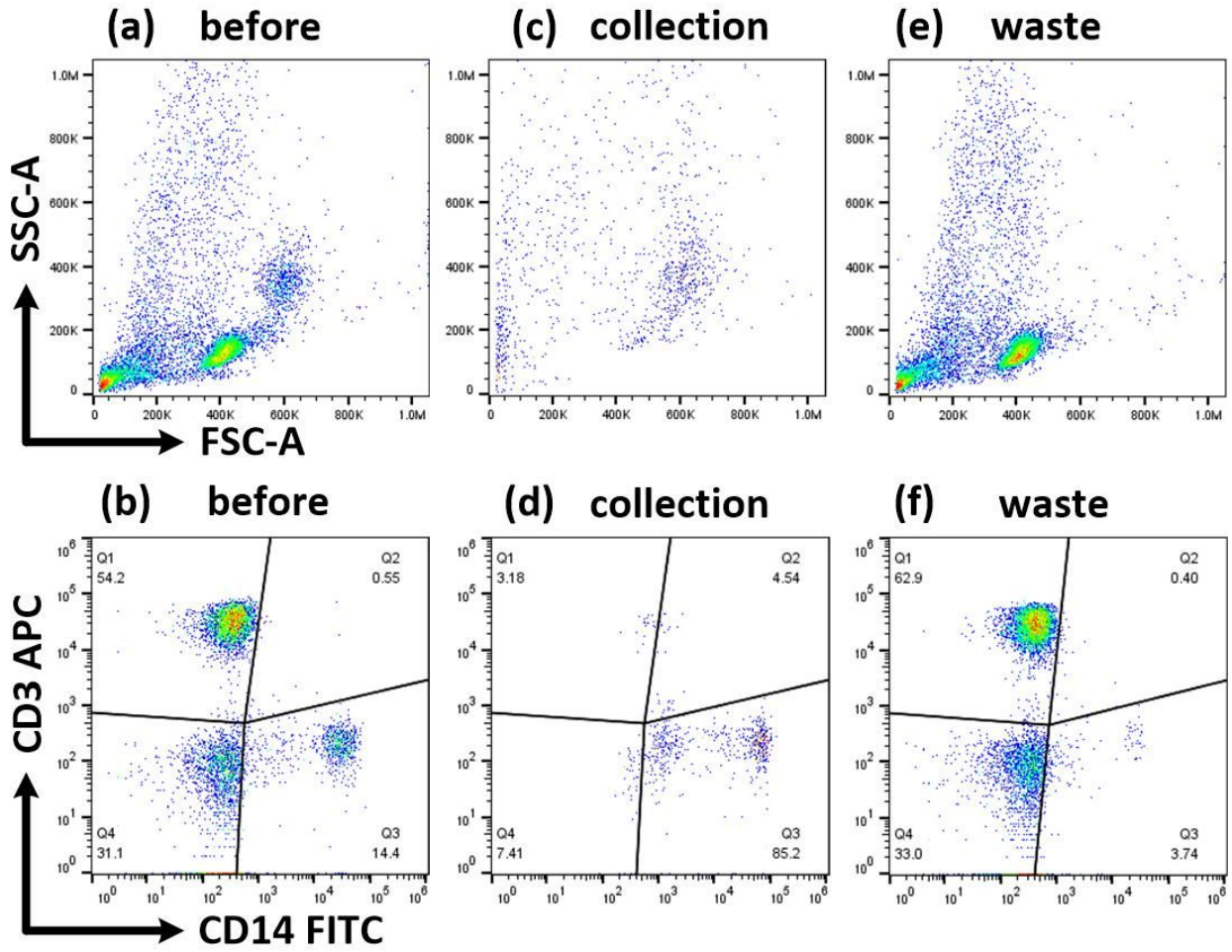

Fig. 7 (a) shows the forward v.s. side scattering plot of PBMC before the TDEP process, in which we can clearly identify three different size distribution, small cells/debri, lymhpocytes, and larger cells. (b) shows that before the separation, 54% of the population was T lymphocytes, 14.4% of the population was monocytes, and the rest 31.1%of the population could include B lymphocytes and natural killer cells. (c) shows the forward v.s. side scattering plot of the sample collected from the collection channel, in which the small cells/debri and lymphocyte population were obviously eliminated. (d) shows the flow cytometer data of the sample collected from the collection channel of TDEP device. The monocyte population (CD14+) was increased from 14% to 85%, which has around 9 fold enrichment. (e) shows the forward v.s. side scattering plot of the sample collected from waste channel, in which retained the population of small cells/debri and lymhpocytes. (f) shows the sample collected from waste channel retained the population of most CD14- cells.